IOP Publishing Nano Futures 8 (2024) 035001 https://doi.org/10.1088/2399-1984/ad70e6

NANO FUTURES

PAPER

The use of orthogonal analytical approaches to profile lipid nanoparticle physicochemical attributes

Callum G Davidson[1], Rand Abdulrahman[1], Panida Punnabhum[1], Michael Cairns[1], Nicholas J W Rattray[1], Robin Capomaccio[2], Kevin Treacher[2], Yvonne Perrie[1] and Zahra Rattray[1,*]

[1] Strathclyde Institute of Pharmacy and Biomedical Sciences, University of Strathclyde, Glasgow, United Kingdom
[2] New Modalities and Parenterals Development, Pharmaceutical Technology & Development, Operations, AstraZeneca, Macclesfield, United Kingdom
* Author to whom any correspondence should be addressed.

E-mail: zahra.rattray@strath.ac.uk

Keywords: lipid nanoparticle, metrology, nanomedicine, asymmetric-flow field flow-fractionation

Supplementary material for this article is available online

OPEN ACCESS

RECEIVED
13 June 2024

REVISED
22 July 2024

ACCEPTED FOR PUBLICATION
19 August 2024

PUBLISHED
6 September 2024

Abstract

Lipid nanoparticles (LNPs) have become a major disruptor within the drug delivery field of complex RNA molecules. The wide applicability of prototype nanomedicines has the potential to fill clinical requirements for use against current untreatable diseases. The uptake and implementation of analytical technologies to evaluate these prototype nanomedicines have not experienced similar growth rates, thus hindering the translation of LNPs. Here, we evaluate a model RNA-LNP formulation with a selection of routine and high-resolution orthogonal analytical techniques across studies on the manufacturing process parameter impact and formulation stability evaluation under refrigerated and ultra-low temperatures. We analysed a model cationic RNA-complexed LNP formulation via the process impact on formulation critical quality attributes, short-term refrigerated stability evaluation and frozen-storage stability using zetasizer dynamic light scattering and nanoparticle tracking analysis. We also evaluated freeze-/thaw-induced stress on LNP formulation using high-resolution field-flow fractionation. Statistical analysis and correlations between techniques were conducted to further enhance our understanding of LNP formulation design and its physicochemical attributes to facilitate LNP formulation clinical translation.

1. Introduction

Lipid nanoparticles (LNPs) as nanocarriers for the delivery of oligonucleotide-based therapeutics have sparked a profound change in the industry sector, due to their success in delivering vaccines during the COVID-19 pandemic. The successful global implementation of LNPs has seen a rapid growth in research into their applications for the delivery of cargo in a range of therapy areas of unmet clinical need. Alterations in LNP constituent lipids and ratios have led to the discovery of a broad spectrum of prospective nanomedicine candidates in pharmaceutical industry pipelines, increasing the popularity of LNPs and their versatility and applicability to a diverse molecular portfolio [1–5].

The successful clinical and commercial translation of LNPs for oligonucleotide delivery depends on acceptable formulation physicochemical stability of the nanocarrier during its shelf life, and the ability to protect oligonucleotide cargo from premature degradation. Highlighted by recent reviews [6, 7], there is a critical need for the development of orthogonal analytical pipelines to profile prototype LNP physicochemical attributes during early formulation development stages. Once manufactured, the LNP formulation critical quality attributes (CQAs) are quantified using established techniques, such as dynamic light scattering (DLS: size and polydispersity), electrophoretic light scattering (ELS: zeta potential) and the RiboGreen™ assay (drug encapsulation efficiency and recovery) [8–10].

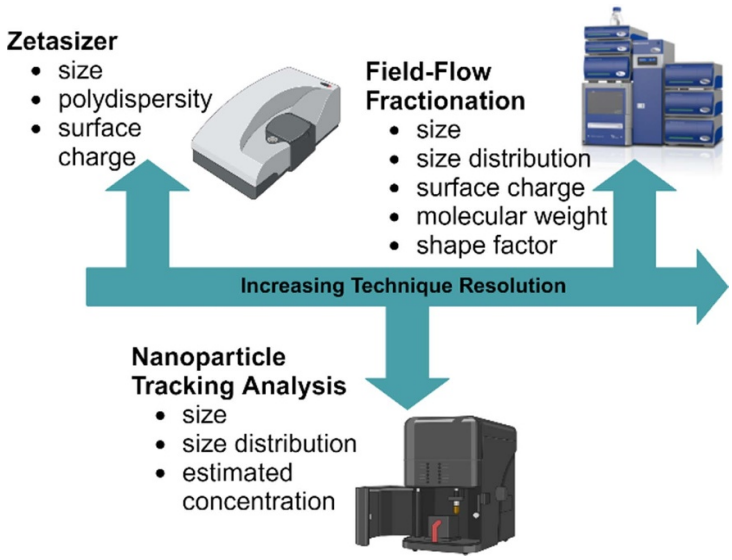

Figure 1. Analytical techniques used in this study for the characterisation of lipid nanoparticles in order of increasing resolution, annotated with respective CQAs.

Due to significant research interest and field novelty, the characterisation of prototype LNP candidates remains on a case-by-case basis. Continuing the process to harmonise the measurement of LNP physicochemical attributes, the Nanotechnology Characterisation Laboratory (NCL) and European NCL have issued guidelines for the analysis of prototype nanoparticulate formulations [11–13]; they recommend the use of at least one low-resolution technique and an orthogonal high-resolution technique for the measurement of nanoparticle size, ensuring that robust and representative results are obtained while standardised reference materials are under development. LNPs are composed of five main excipients: (i) the oligonucleotide active pharmaceutical ingredient [14, 15], (ii) an ionisable/cationic main lipid [16–18], (iii) sterols [16–18], (iv) helper phospholipids [19, 20], and (v) polyethylene glycol functionalised lipids [21–23].

Orthogonal analytical techniques measure equivalent CQAs via differing physical principles. While LNP research has seen significant growth, the introduction of novel analytical pipelines has not kept up with advancements in LNP formulation, presenting a translational gap.

In this study, we address this gap by reporting the use of an analytical pipeline for measuring LNP stability using a range of physical techniques spanning the low- to high-resolution analytical space [12] (figure 1).

Trends in the current LNP literature demonstrate decreased adoption of high-resolution analytical techniques in the routine testing of novel LNPs, with DLS remaining as the gold-standard technique (figure 1) for the measurement of size and polydispersity. Nanoparticle tracking analysis (NTA) has emerged as a higher-resolution particle-sizing technique in recent years, where particle size and size distributions are determined on a particle-particle basis in contrast to the bulk light scattering properties of DLS. NTA tracks the movement of particles over a set frame distance to correlate movement velocity with size, and thus size distribution. NTA can also determine the estimated concentration of particles in an LNP formulation. Previous work within the field using a complex nanocarrier system has correlated LNP CQAs with DLS and NTA techniques' main ionisable/cationic lipid [24].

Increasing in measurement resolution beyond DLS and NTA is asymmetric flow field-flow fractionation (AF4), which gently separates complex and labile nanoparticles, and downstream detection of the resolved fractions is achieved using a hyphenated inline multidetector (MD) system. These detectors include, and are not limited to, UV/Vis spectroscopy, multi-angle light scattering (MALS), DLS, fluorescence and the refractive index. By combining different detectors and field-flow fractionation (FFF) modalities (e.g. AF4, electrical AF4, centrifugal FFF), the LNP particle size, size distribution, surface charge, molecular weight and shape factor can be determined simultaneously during a single measurement run. Fractions generated during LNP fractionation can also be collected according to eluted fractions for further offline analysis with additional analytical techniques (e.g. liquid chromatography mass spectrometry).

The techniques discussed here have been used in several studies to characterise complex nanocarriers [25–29], including specialist LNP systems [11, 30–32]; however, to deepen our understanding of CQAs, simpler systems must be used and evaluated through the full manufacturing pipeline from microfluidic, to purification and filtration, refrigerated and frozen (−80 °C) storage conditions. Frozen storage at −80 °C was selected for this work, since the Pfizer/BioNTech COVID-19 vaccine is stored at −80 °C, which is the

lowest commercial freezer temperature prior to liquid nitrogen storage. Final product storage conditions must be incorporated into early development LNP testing to ensure storage suitability. Frozen storage at ultra-low conditions poses supply chain problems, with the transport of LNPs noted during mass immunisation against COVID-19.

In this work we highlight the need for high-resolution techniques to profile LNP candidate physicochemical properties during early nanomedicine development to facilitate translation using model oligonucleotide LNPs. We use 1,2-dioleoyl-3-trimethylammonium-propane chloride salt (DOTAP), as the main ionisable lipid within the formulation due to its permeant cationic charge. Poly(A) is used as a model mRNA oligonucleotide drug encapsulated within LNPs. Both components have been widely used within the field; however, a cross-comparison of techniques has not been attempted to the best of our knowledge using our microfluidics-based manufacture, downstream processing and MD-AF4 setup.

The goal of this study is to develop an orthogonal analytical pipeline to characterise the physicochemical stability of LNPs, using a PolyA DOTAP-LNP prototype as a model example. We report the evaluation of in-process manufacturing steps on LNP physical parameters, and an assessment of their physicochemical stability under refrigerated and ultra-low frozen-storage (−80 °C) conditions.

2. Materials and methods

2.1. Materials

DOTAP, 1,2-distearoyl-sn-glycero-3-phosphocholine (DSPC) and 1,2-dimyristoyl-rac-glycero-3 -methoxypolyethylene glycol-2000 (DMG-PEG2000) were purchased from Avanti Polar Lipids (Alabaster, USA). Cholesterol (CHOL), cellulose dialysis membrane (MWCO 14 kDa), and Poly(A) were purchased from Sigma Aldrich (Merck, Poole, UK). Polyethersulfone (PES) 0.2 μm Acrodisc® filters were purchased from Pall Corporation. DNA-/RNA-free water, ethanol, 10X phosphate-buffered saline (PBS) pH 7.4, polyvinylidene difluoride (PVDF) 0.22 μm filters, Quant-iT™ RiboGreen™ RNA Assay Quantitation Kit (R4110), and sodium citrate dihydrate were acquired from ThermoFisher (Fisher Scientific, Leicestershire, UK). All solvents and other chemicals used were of analytical grade, and milliQ-water (18.2 Ω cm^{-1}) was provided by an in-house system.

2.2. Manufacture of PolyA-DOTAP-LNPs

LNPs were formulated on the NanoAssemblr® IgniteTM Platform (Precision Nanosystems Inc, Vancouver, BC, Canada) in toroidal micromixer single-use cartridges (Ref: NIN0002). The system channel was 300 μm wide with a height of 130 μm [33]. The LNP prototype was composed of DOTAP:CHOL:DSPC:DMG-PEG2000. All initial lipid stock solutions were prepared in ethanol at 5 mg ml^{-1} and combined in a 50:38.5:10:1.5 molar ratio for cationic lipid:cholesterol:helper:PEG-lipid, respectively, based on Onpattro® and Comirnaty® formulations [34]. Poly(A) was prepared in DNAse-/RNAse-free water at 1.5 mg ml^{-1} and diluted in citrate buffer pH 6 (50 mM), which was used as the aqueous phase. The lipid organic phase and PolyA aqueous phases were injected simultaneously into the micromixer in a 3:1 aqueous:organic flow rate ratio (FRR), 15 ml min^{-1} total flow rate (TFR) with an N:P ratio of 6:1. The final lipid theoretical concentration after microfluidic preparation was 1.25 mg ml^{-1}, with a corresponding theoretical PolyA concentration of 0.055 mg ml^{-1}. Newly formulated PolyA DOTAP-LNPs were dialysed against filtered 1 × PBS (pH 7.4) (X200 dialysate ratio) to remove residual ethanol/citrate buffer. Dialysis was performed using a cellulose dialysis membrane (MWCO 14 kDa) at ambient temperature for 1 h under magnetic stirring using an established method [9].

2.3. Stability testing of prototype LNPs

2.3.1. Process parameter testing of LNPs

LNPs were tested at various stages throughout the manufacturing process pipeline, including post-microfluidics manufacture, post-dialysis purification and post-filtration (PES and PVDF filtration).

2.3.2. Stability testing of refrigerated LNP formulations

LNP aliquots were stored at 4 °C from the day of manufacture (day 0) to one month (day 28).

2.3.3. Stability testing of lipid nanoparticle (LNP) formulation at ultra-low temperature (−80 °C)

LNPs were manufactured and buffer-exchanged via dialysis into a frozen-storage buffer containing various sucrose concentrations for use as a cryoprotectant. Sucrose was added at 0% (PBS control), 5%, 10% and 20% (w/v) concentrations to the dialysis buffer (PBS). All LNP samples were analysed on the day of manufacture (day 0) and following 1 × freeze/thaw (F/T) cycle from −80 °C to ambient temperature.

2.4. Characterisation of LNP formulations

2.4.1. Dynamic light scattering

Particle size (Z-average) and the polydispersity index (PDI) were measured by DLS using a Zetasizer Nano ZS system (Malvern Panalytical, Worcestershire, UK) equipped with a 633 nm helium–neon laser and a detection angle of 173° (non-invasive back scattering). Unless otherwise stated, all measurements were performed at 25 °C and at a 1:10 dilution in PBS (pH 7.4) for all LNP samples, to achieve a final theoretical lipid concentration of 125 μg ml^{-1} (corresponding theoretical PolyA concentration-5.50 μg ml^{-1}). All measurements were performed in three independent replicate measurements consisting of at least two technical replicates.

2.4.2. Electrophoretic light scattering

The LNP ζ-potential surface charge was measured using an ELS post-manufacture/process test. Unless otherwise stated, all measurements were performed at 25 °C and at a 1:10 dilution in DNA-/RNA-free water established in [9] for all LNP samples, to produce a final lipid theoretical concentration of 125 μg ml^{-1} (the corresponding theoretical PolyA concentration was 5.50 μg ml^{-1}). All ζ-potential measurements were performed using three independent replicate measurements consisting of at least two technical replicates.

2.4.3. Nanoparticle tracking analysis

Particle sizes, particle size distribution and estimated concentration were measured by NTA using a NanoSight NS300 system (Malvern, Worcestershire, UK), equipped with a low-volume flow cell, a 488 nm laser, an automated syringe driver and a sCMOS camera. All samples were diluted in PBS (pH 7.4) prior to analysis with NTA (dilutions are noted in table S1); dilutions vary due to LNP recovery post-dialysis and experimental testing.

All measurements were performed at 25 °C and injected into the flow cell using a syringe driver set at an infusion rate of 50. The corresponding NTA data acquisition parameters were five replicate videos of 60 s duration and a camera level of 15. All data were analysed in the NTA 3.4 Build 3.4.003 program with a detection threshold set to five. Three independent replicate measurements consisting of five technical replicates each were performed for each sample.

2.4.4. Frit-inlet (FI) asymmetric flow field-flow fractionation (AF4)

An AF2000 AF4 module (PostNova Analytics, Germany), hyphenated with MD multi-angle light scattering (MALS-PN3621, PostNova Analytics), a UV detector (PN3242, 280 nm- PostNova Analytics) and a DLS Zetasizer Nano ZS system (Malvern Panalytical, Worcestershire, UK), was used to perform the separation and inline analysis of model LNPs. An FI channel, with a channel spacer thickness of 350 μm, and a 10 kDa molecular weight cut-off (MWCO) size amphiphilic regenerated cellulose membrane was used, with a 100 μl sample injection loop, and an injection volume of 20 μl. PBS (pH7.4) was used as the eluent buffer, and a corresponding injection flow rate of 0.2 ml min^{-1}, cross-flow rate of 0.75 ml min^{-1} (exponential power decay 0.2) and a detector flow rate of 0.3 ml min^{-1} were used as the elution conditions. The channel membrane was conditioned with triplicate injections of bovine serum albumin (BSA) (5 mg ml^{-1}) and five injections of fresh LNPs (0.5 mg ml^{-1}). Each LNP sample was injected in technical replicates of four (0.5 mg ml^{-1}). LNP recovery (% Rec) was calculated by integrating the UV area under the curve (AUC) from direct injection (cross-flow = 0 ml min^{-1}) and the cross-flow applied (0.75 ml min^{-1}) area under the UV curve, using equation (1),

$$\%\text{Recovery} = \frac{\text{AUC}_{\text{direct injection}}}{\text{AUC}_{\text{cross - flow separation}}} * 100$$

Calculation determining recovery of LNPs using UV integrated AUC from LNP direct injection and cross - flow applied separation profile. (1)

Data were analysed in the Nova FFF software version 2.2.0.1 (PostNova Analytics, Landsberg, Germany) using the MALS spherical model for fresh day 0 LNPs and a random coil for stress-induced freeze/thaw LNPs.

2.4.5. Quantification of encapsulation efficiency and mass balance

The encapsulation efficiency (EE, equation (2)) and drug recovery (mass balance, MB, equation (3)) of the Poly(A) cargo during LNP formulation were measured using the Quant-iT™ RiboGreen™ RNA Quantitation assay kit (Thermo Fisher #4110) and used as per manufacturer's instructions. The kit quantifies the total RNA and unentrapped RNA on the outside of the LNP to calculate the efficiency of drug encapsulation during formulation. The assay also determines recovery by comparing the total RNA of the

formulation to a theoretical RNA concentration,

$$\%\ \mathrm{EE} = \frac{\mathrm{Total}_{\mathrm{drug}} - \mathrm{Free}_{\mathrm{drug}}}{\mathrm{Total}_{\mathrm{drug}}} * 100$$

Calculation determining encapsulation efficiency (drug loading) of encapsulated oligo drug. (2)

$$\%\ \mathrm{MB} = \frac{\mathrm{Total}_{\mathrm{drug}}}{\mathrm{Theoretical\ Concentration\ of\ Drug}} * 100$$

Calculation determining mass balance (drug recovery) of encapsulated oligo drug. (3)

The corresponding fluorescence intensity of the RiboGreen™ signal was measured on a GloMax® Explorer GM3500 microplate reader (Promega, UK) at an excitation wavelength of 475 nm, with the emitted fluorescence measured at 500–550 nm. All fluorescence data were captured at ambient temperature (25 °C) using GloMax® firmware version 4.29.0 and processed using GloMax® Fluorescence software version 3.1.0.

2.5. Statistical analysis

The corresponding mean ± standard deviation (SD) was calculated for all experiments with a minimum of two independent and two technical replicates, unless otherwise stated. A one-way analysis of variance (ANOVA) was performed to compare and highlight the impact of process parameters and stability on prototype LNP formulations. Statistical analyses were performed using Minitab® version 20.4 software. Data were graphed using OriginPro version 9.9.0.220. Unless otherwise specified, no significant differences were noted between evaluated conditions, where $^{*}p < 0.05$, $^{**}p < 0.005$, $^{***}p < 0.0005$.

3. Results

3.1. PolyA-DOTAP-LNP process parameter impact on formulation CQAs

Firstly, we investigated the influence of key LNP manufacturing process parameters on the measured attributes from samples collected during the initial microfluidics manufacture, formulation purification and sterile filtration using two common filtration membranes, PES and PVDF. Samples collected from each process step were characterised using pipeline assays developed and standardised in our labs, consisting of Zetasizer, NTA and RiboGreen™.

The process parameter impacts on PolyA-DOTAP-LNPs (figures 2, S1 (A), (B), tables S2 and S3) demonstrate similar trends in size and size distribution (∼60 nm) with lower particle size measured via PDI/NTA span values for all measured in-process stages, excluding PVDF-filtration. Dialysis and PES filtration steps highlighted higher reproducibility with minimal aggregates and sub-populations in comparison to the PVDF filtration step. PVDF-filtered LNPs exhibited the largest particle size, the highest measured PDI, the lowest surface charge and lowest encapsulation efficiency and mass balance. The mass balance indicated the minimal drug recovery post-filtration process, of which 70% of the PolyA was encapsulated and 30% was free (table S2).

Collectively, by combining CQAs and cross-comparison of the post-dialysis and PES filtration stages, we hypothesise that PVDF filtration resulted in the loss of DOTAP lipid-PolyA drug electrostatic complexes due to membrane adsorption, resulting in aggregation and particle self-association leading to a 110% increase in size (115.7 nm versus 56.9 nm post-PES filtration).

Size distribution measurements, the PDI and NTA span increase in value with each succeeding process step. The PDI increased by 23% from post-microfluidic (0.13) manufacture to post-PVDF filtration (0.16), whereas the NTA span increased by 66% (0.27) from post-microfluidic manufacture to post-PVDF filtration. These increased shifts in size distribution indicate detectable sub-population formation with each process parameter compared with post-microfluidic manufacture as expected, as manufacturing buffer is removed and filtration stress/strain impact on LNP integrity. DLS highlights the main changes in PDI via size distribution intensity (figure S1 (A)) for PVDF filtration, whereas a larger difference in size distribution is visualised (figure 2(D)) and noted (table S3) for NTA span. Post-dialysis and post-PES conditions produce size distributions which are not significantly different, showing PES membrane suitability for LNP filtration post-dialysis purification.

The post-manufacture buffer contains 25% ethanol and 75% citrate buffer (37.5 mM sodium citrate pH 6.0). At pH 6.0, citrate is deprotonated at two carboxyl groups [35], resulting in an electrostatic attraction with the cationic surface of LNPs, thus masking the surface potential charge and lowering zeta potential measurements. Alternatively, unencapsulated PolyA could be bound loosely to LNP surface

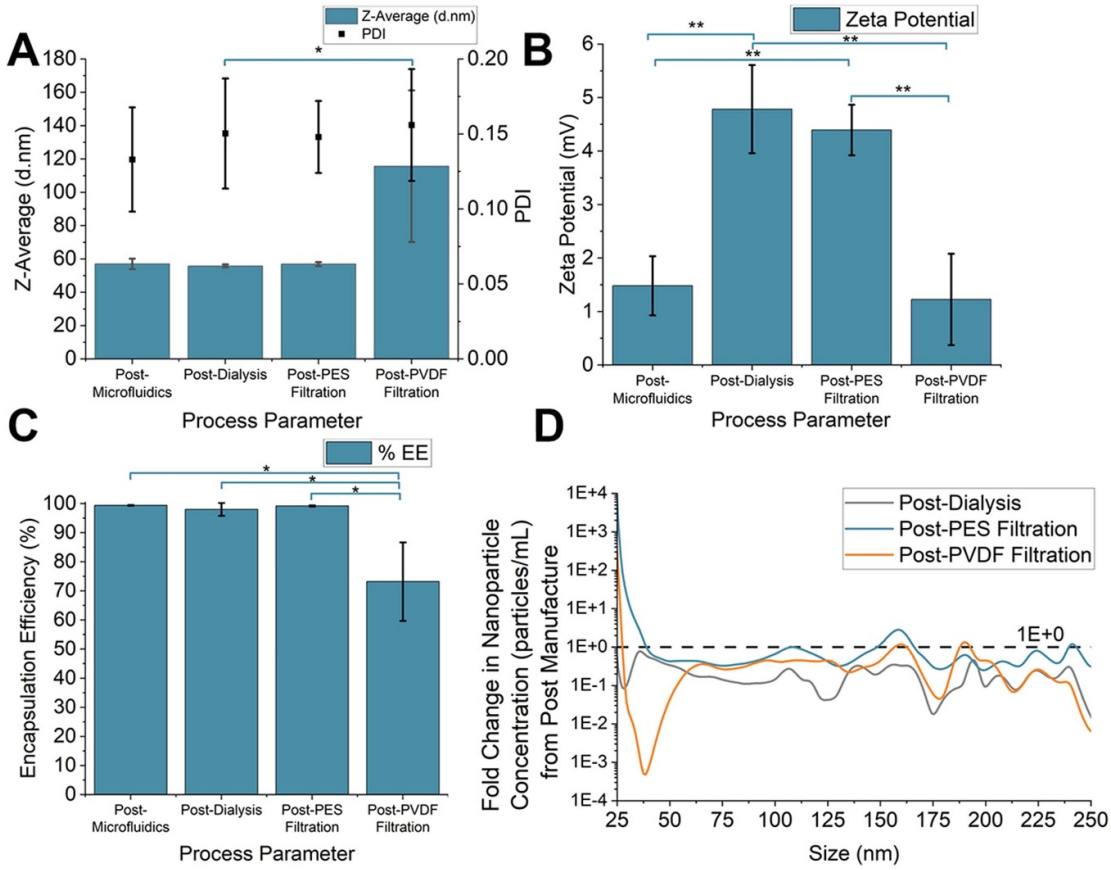

Figure 2. Physicochemical trend analysis of the process parameter impact on PolyA-DOTAP-LNPs using (A) (5.50 μg ml^{-1} PolyA) DLS to measure the size and polydispersity index (PDI), (B) (5.50 μg ml^{-1} PolyA) ELS for measurement of the zeta potential, (C) (0.75 μg ml^{-1} PolyA) the encapsulation efficiency (%EE) assay, and (D) NTA for the mean and mode size (table S1 for PolyA conc.) normalised against post-microfluidics, (mean $\pm$ SD, $n = 3$), one-way ANOVA Tukey test comparing each process parameter per CQA, $^{*}p < 0.05$, $^{**}p < 0.005$ and $^{***}p < 0.0005$.

post-microfluidics, lowering the surface charge. With the removal of manufacturing buffer post-dialysis purification with PBS, we note an increase in surface charge, potentially removing loosely bound PolyA. The PDI also increased in post-dialysis samples, showing sub-population formation with the removal of manufacturing buffer conditions. The PDI measured for post-microfluidic to post-dialysis samples increased, which was accompanied with a decrease in size due to citrate molecule removal from smaller particles, noting dialysis within a detectable range, increasing the PDI but reducing the overall size.

The mass balance of PolyA (table S2) from the formulation decreased by ~25% (68.7%) following dialysis into PBS and remained at ~65% post-PES filtration, demonstrating that PES filtration had minimal impact on the measured formulation characteristics.

The NTA estimated particle concentration varied at each process stage, with the highest measured particle concentration post-manufacture, as expected, due to the lack of further downstream processes, whereas dialysis and filtration both impacted the overall estimated particle concentration measured by NTA (figure S1(B)). With dilutions decreasing from 10,000-fold to 100-fold, a 72% decrease in the estimated concentration from post-microfluidic manufacture to post-PVDF filtration was observed.

3.2. PolyA-DOTAP-LNP short-term physicochemical stability evaluation

We evaluated the physical stability of DOTAP-LNPs over a 28 day period by analysing formulation CQAs using DLS, NTA and the RiboGreen™ assay. day 0 refers to the day of manufacture. Formulations were analysed post-dialysis, without filtration and stored in glass vials under refrigerated conditions.

Across the 28 day stability study, all measured CQAs exhibited time-dependant changes as measured (figure 3, table S4, S2 (A) (B), and table S5). DLS size and PDI (figure 3(A)) show changes in size and size distribution across the study. DLS size increased by 14 nm from day 0 to day 28, with significantly different average-size LNPs on day-7 compared to day 0. Changes in the z-average could be attributed to DLS bias towards larger particles, consistently resulting in larger measured sizes. With the increased particle size, the

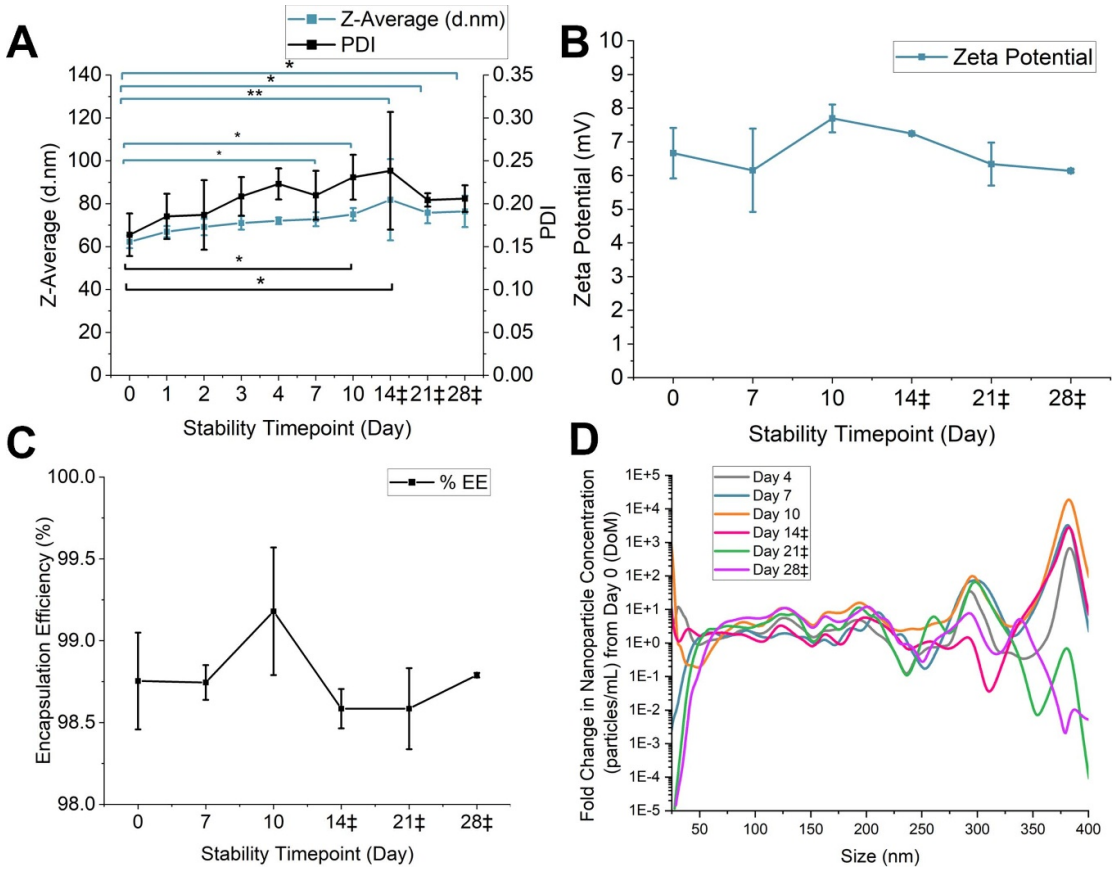

Figure 3. Physicochemical trend analysis of the refrigerated (4 °C) storage stability impact on PolyA-DOTAP-LNPs using (A) (5.50 μg ml^{-1} PolyA) DLS to the measure size and polydispersity index (PDI), (B) (5.50 μg ml^{-1} PolyA) ELS for measurement of the zeta potential, (C) (0.75 μg ml^{-1} PolyA) the encapsulation efficiency (%EE) assay, and (D) NTA for the mean and mode size normalised against Day 0 (table S1 for PolyA conc.) (mean ± SD, ‡$n = 2$, $n = 3$), one-way ANOVA Dunnett test comparing each time point with day 0 CQAs, $^{*}p < 0.05$, $^{**}p < 0.005$ and $^{***}p < 0.0005$.

size distribution remained similar to previous and subsequent day analysis (∼0.2) (table S4). Comparisons of size distributions (figure S2 (A)) showed an increase in aggregate detection intensity on day 10 and day 14 relative to day 0, thus increasing polydispersity measurements.

The measured zeta potential surface remained cationic within +6–8 mV with no significant differences noted over the measured time points (table S4). Changes in surface charge could be due to the conformation of the DOTAP lipid within the formulation migrating towards a more thermodynamically favourable position on the outer surface of the LNP, thus producing varied cationic surface charges compared to day 0 LNPs. PolyA encapsulation remained high (>98%) throughout the 28 day evaluation, highlighting that no PolyA leaked from the formulation over the stability period, and that PolyA remained in a thermodynamically favourable position within the LNP complex (table S4). PolyA recovery was also high on day 0 (>60%).

The NTA data produced varying results over the analysed stability period (figure 3(D)) for mean, mode and span values, indicating (figures S2 (A) and (B)) sub-population formation. Subsequent time-point analysis (day 14, −21, and −28) showed increasing mean and mode sizes with variable associated span values. Decreases in size distributions >325 nm were noted for day 21 and day 28 time points (figure 3(D)), highlighting a narrower size distribution than previous time points. Narrowed size distributions are confirmed through decreased PDI and NTA span values (table S5-5). As with DLS data denoting significant differences in size and PDI data, equivalent statistical differences on evaluated stability time points were not produced within the NTA analysis. Contrasting results between low- and high-resolution techniques indicate the need for higher-resolution analytical techniques for CQA evaluation.

3.3. PolyA-DOTAP-LNP frozen-storage physicochemical stability evaluation

With a vast array of cryoprotectants available for use in frozen storage of LNPs, we focused on sucrose inclusion as the cryoprotectant used in the Moderna and Pfizer/BioNTech COVID-19 vaccination storage buffers [36]. LNPs were manufactured and dialysed into PBS (pH 7.4) containing sucrose at different

concentrations (% w/v). LNPs were stored and frozen in DNAase-/RNAase-free low-protein binding microcentrifuge tubes at −80 °C and subjected to a single freeze/thaw cycle at ambient temperature.

Overall, the inclusion of sucrose in the formulation storage buffer impacted the measured LNP CQAs (figure 4, table S6, figure S3 and table S7).

The post-manufacture/purification day 0 measurements align with previous data for day 0 samples. Across all the sucrose concentrations studied on day 0, the particle size and PolyA encapsulation efficiency measurements were reproducible. Irrespective of the sucrose concentration used, a decrease in surface charge was noted with an ∼30% reduction in the measured zeta potential, correlating with an increase in the formulation buffer sucrose concentration of PolyA recovery. An increase in PolyA recovery (16%) was noted when the sucrose concentration was increased to 20% (w/v), which was accompanied by a reduction in the PDI and NTA span, highlighting a decrease in the measured particle size.

The measured z-average, PDI, NTA mean, mode and span CQAs increased with induced stress from the freeze/thaw cycling process, highlighted by figures 4(A)–(H) and S3. Sucrose disrupted the formation of ice crystals as the size distribution and NTA span decreased with increasing sucrose content post F/T, PDI < 0.45 and NTA span < 1.3.

A comparison of DLS and NTA data following LNP exposure to freeze/thaw stress highlights vast differences in the technique results and CQAs, highlighting the need for in-depth high-resolution analytical methodology and evaluation. To further probe the colloidal stability in the absence of a cryoprotectant, we developed and employed FI-AF4 and inline hyphenated UV-MALS-DLS MD methodology to evaluate the impact of F/T stress on LNP attributes.

3.4. FI-AF4-MD evaluation of PolyA-DOTAP-LNPs

Here, we developed an analytical pipeline for the evaluation of PolyA-DOTAP-LNP colloidal stability after freeze/thaw stress in the absence of a cryoprotectant. For corresponding information on the method simulated elution profiles, (figure S4), ISO performance criteria are noted in the supplementary information (table S8). LNPs were manufactured and dialysed into formulation buffer (section 2.2) and analysed using FI-AF4-UV-MALS-DLS. LNPs (0% sucrose) from frozen stability were thawed to ambient temperature from −80 °C prior to analysis.

From high-resolution AF4 data, two batches of LNPs were analysed on day 0 demonstrating inter-batch variation in the manufacturing process at a small scale. Identical formulation process steps were followed for each batch manufacture, producing two distinct sized batches of LNPs, highlighting manufacturing variability. The elution profile retention times observed at 26 and 21 min for LNP1 and LNP2 batches correspond to cross-flow decay flow rates of 0.216 ml min^{-1} and 0.277 ml min^{-1}, respectively. Changes in retention time were noted in figures 5(A) and (B) with corresponding UV (280 nm) and MALS 90° detector signals. Both figures highlight a decrease in detector signal intensity, with the LNP1 batch producing a higher UV signal (29%) and MALS signal (47%) than the LNP2 batch. Although both LNP batches produced varying retention times, detector signal intensities, radius of gyration and hydrodynamic radius, the shape factor remained consistent at 1, highlighting that both batches have similar morphology, changing throughout the elution profile from 15 to 40 min (figure 5(C)). A high AF4 LNP recovery (>97%) shows minimal LNP–membrane interactions, meeting the ISO standard performance criteria for an AF4 technique (tables 1 and S8). The size distributions denote that the LNP1 batch led to a more polydisperse population distribution, highlighted by a broader peak profile and reduced signal intensity in comparison to the LNP2 batch, which produced a narrower and more intense peak (figure 5(D)).

Freeze/thaw stressed LNPs aggregated extensively as expected from the DLS/NTA data with enhanced visual turbidity and precipitation. LNPs produced a retention time of 56 min, suggesting a change in structure/size with a corresponding cross-flow flow rate of 0.055 ml min^{-1}, suggesting poor size separation. The UV detector produced a minimal signal (>0.2 mV), less than the void peak signal (1 mV) (figure 5(E)), and the MALS detector produced a signal around 0.37 mV, demonstrating LNP aggregates scatter less light in comparison to fresh LNPs (figure 5(F)). Further confirmation of poor separation and detection was confirmed with low UV-MALS detector signals, which aligned with a low inline DLS signal with detector intensity < 40 kcps. The radius of gyration and hydrodynamic radius data highlight a vast difference in detector sensitivity and poor recovery of LNPs following F/T (13%, table 1) as fresh LNPs produced a shape factor of ∼1. At sizes >1 μm, non-Brownian movement forces dominate; therefore, larger particles are unsuitable for DLS detection. Hence, large hydrodynamic radii were noted for FT Rep1 (figure 5(G)). F/T LNP replicates produced varying shape factors. Our data highlights the aggregation analysis variability within sample technical replicates and between independent sample replicates. A large size distribution was noted in figures 5(G and (H) with a broad and flat distribution. Countless studies have aimed to prevent aggregation within LNP formulations in frozen-storage conditions; however, little is known about the

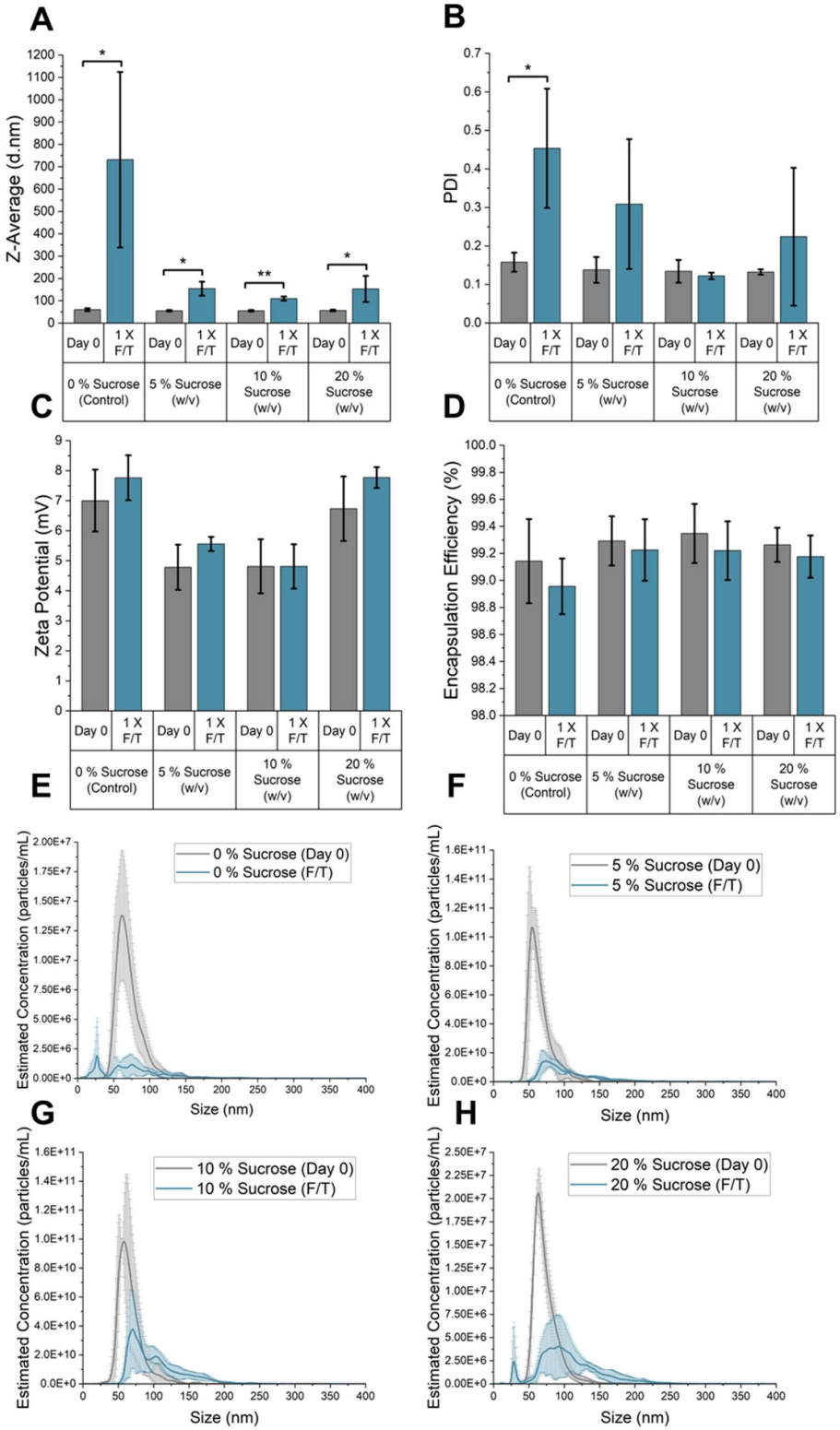

Figure 4. physicochemical trend analysis of the frozen-storage stability of PolyA-DOTAP-LNPs formulated with 0%, 5%, 10% and 20% sucrose (w/v) cryoprotectant on Day 0 (day of manufacture) and after 1 × freeze/thaw cycle (1 × F/T) from −80 °C to ambient temperature. DLS was used to measure (A) size and (B) the polydispersity index (PDI) (5.50 μg ml^{-1} PolyA). (C) ELS was used to measure the zeta potential (5.50 μg ml^{-1} PolyA), and (D) RiboGreen™ for PolyA encapsulation efficiency measurement (0.75 μg ml^{-1} PolyA), and NTA for (E) 0% sucrose, (F) 5% sucrose, (G) 10% sucrose and (H) 20% sucrose storage buffer on day 0 and post freeze/thaw (table S1 for PolyA conc.) (mean ± SD, n = 3), one-way ANOVA Dunnett test comparing each time point with day 0 CQAs per individual sucrose concentration condition, $^{*}p < 0.05$, $^{**}p < 0.005$ and $^{***}p < 0.0005$.

physical/mechanical aggregation formation of LNP formulations. Due to high intra-sample and inter-sample variability and overall low recovery, the hydrodynamic radius, radius of gyration and shape factor ratio were used to demonstrate LNP CQA changes and the consequent AF4 analytical impact.

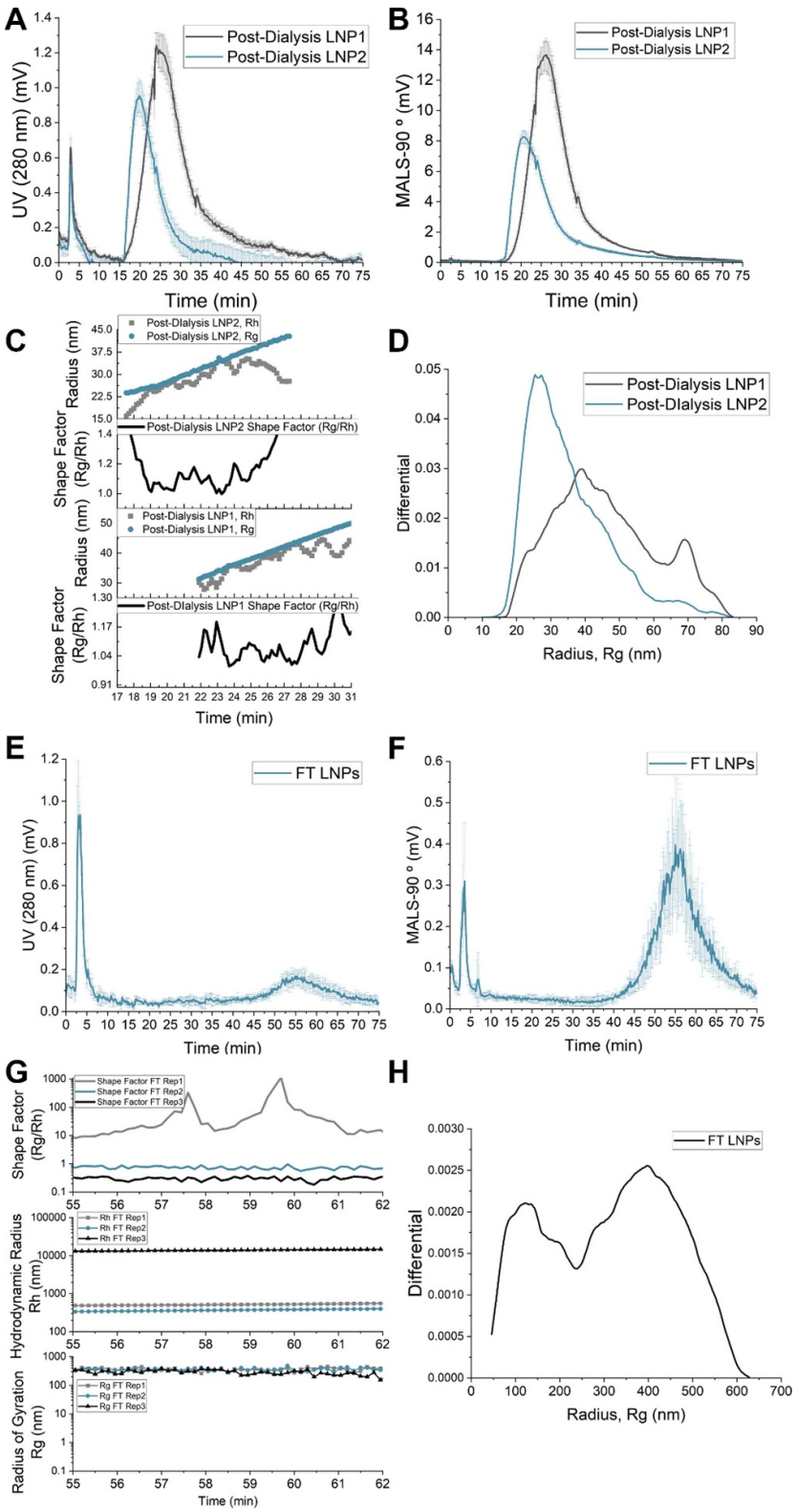

Figure 5. FI-AF4-MD evaluation of PolyA-DOTAP-LNPs post-dialysis: (A) the UV elution profile, (B) the MALS elution profile, (C) the shape factor (Rg/Rh) and (D) size distribution ($n = 1$, mean of triplicate injections ± SD). Evaluations of freeze/thaw cycled PolyA-DOTAP-LNPs: (E) the UV elution profile, (F) the MALS elution profile, (G) the shape factor (Rg/Rh) and (H) size distribution (A, B, E, F, $n = 3$, mean of triplicate injections ± SD, C, D, G H, $n = 1$, mean of triplicate injections).

As NTA and AF4 are high-resolution techniques, table 1 cross-compares mode LNP sizes for each condition. The particle size measured for LNPs analysed on day 0 yielded the most comparable values across all the techniques. In contrast, the measured aggregate size distributions varied between techniques, due to the low recovery from AF4, whereas all the LNPs were recovered from NTA analysis.

Table 1. Cross-comparison of mode PolyA DOTAP-LNP formulation size between high-resolution orthogonal NTA ($n = 3 \pm$ SD) and FI-AF4-MD techniques. ET: elution time ($n = 3$ injections $\pm$ SD).

	NTA	FI-AF4-MD		
Sample type	Mode size (nm)	ET (min)	Mode size (nm)	Recovery (%)
Day 0, LNP batch 1	61.4 ± 7.4	26	78.8 ± 1.0	97.1 ± 7.9
Day 0 LNP batch 2		21	58.1 ± 0.3	97.3 ± 5.7
1 × F/T cycled, PolyA DOTAP-LNP	62.7 ± 15.4	56	831.6 ± 92.0	13.8 ± 1.9

3.5. Overall correlation of PolyA DOTAP-LNP CQAs between analytical assays

From the overall pipelines demonstrated within this study, we have analysed the correlation between CQAs using Pearson correlation. Samples that were also included in the correlation matrix were from the day of manufacture (day 0), post-dialysis without filtration. To successfully correlate CQAs, data assumptions were followed: (1) the measured CQAs must be measured at the continuous level; (2) a linear relationship must exist between CQAs; (3) CQAs must contain no significant outliers; and (4) CQA measurements must be normally distributed using the Shapiro–Wilk normality test. All the CQA data satisfied these assumptions; however, a single replicate of encapsulation efficiency from a manufacturing process parameter study was removed as a statistical outlier.

From the visualisation of each individual replicate from each study (figure 6(A)), it was noted that the evaluated pairwise-CQAs do not cluster per study, highlighting the variability within small-scale manufacturing and purification of LNP formulations. Variability in clustering also demonstrated batch-to-batch differences in LNPs. Also, although tight clustering between study replicates was not visualised, the ranges of measured CQA values remained low with the CQA that produced the smallest variable range having a 1% difference between the highest and lowest PolyA encapsulation efficiencies, and the largest variation being a surface zeta potential at 88% between study replicates' highest and lowest values. Grouping all study day 0 measured LNP replicates has produced generic trends of visualised CQA values with average-sized particles around 60 nm, low size distribution (PDI < 0.2), near-neutral cationic surface charge (+6 mV) and high encapsulation efficiency (>95%), and mass balance (>60%).

The linear correlation weightings (figure 6(B)) show how strongly two observed LNP CQAs are positively correlated, negatively correlated or neutrally correlated. Anti-correlations (<0) indicated an increase in the CQA value for one characteristic with a reduction in the opposite CQA measurement; whereas positive correlations (>0) indicated an increase in one measured CQA value and an increase in the other measured CQA value. The matrix highlighted techniques measuring particle size and size distributions produced more positive linear correlations (Z-average, NTA mode/mean/span) with each other, with higher positive correlations extended from analytical techniques used to evaluate both CQAs being compared (NTA mean/mode, DLS z-average/PDI). The PDI produced neutral correlation values compared with the zeta potential and NTA CQAs. PolyA drug encapsulation/recovery CQAs produced negative correlations between zetasizer and NTA-evaluated CQAs, with only a positive correlation noted between both the encapsulation efficiency and mass balance (figure 6(B)). Both negative correlations highlight maximal PolyA drug loading and recovery with smaller particle sizes and near-neutral surface charge.

The matching correlation strength, the statistical significance of pairwise correlations, is shown in figure 6(c). Statistically significant linear correlations produced a weighting of >0.6, equalling a p-value <0.05, with a weight of 0.98 matching a calculated p-value <0.0005. Both sets of p-values denote statistically significant linear relationships between Z-average/PDI and NTA mean/mode size, with both measured CQAs originating from the same analytical instrument; whereas PolyA encapsulation efficiency/NTA produced a significantly linear relationship between both CQAs, highlighting inter-technique anti-correlation and a statistically significant linear relationship. As the encapsulation efficiency (EE%) increased, the NTA span decreased, meaning LNP formulations with higher drug encapsulation, also containing smaller size distributions measured through NTA. Incorporating the correlative strength of measured CQAs and statistical significance within particle evaluation is a necessary step to obtain a deeper understanding of LNP CQAs to understand physicochemical parameter behaviour and connections between measured characteristics.

4. Discussion

Interest in the use of LNPs as a drug delivery platform for gene delivery has seen an exponential increase over the past decade, with the regulatory approval of three LNP-based nanomedicine products: one therapeutic, and two vaccines for use in clinical settings. Since oligonucleotides encapsulated in LNPs can consist of a

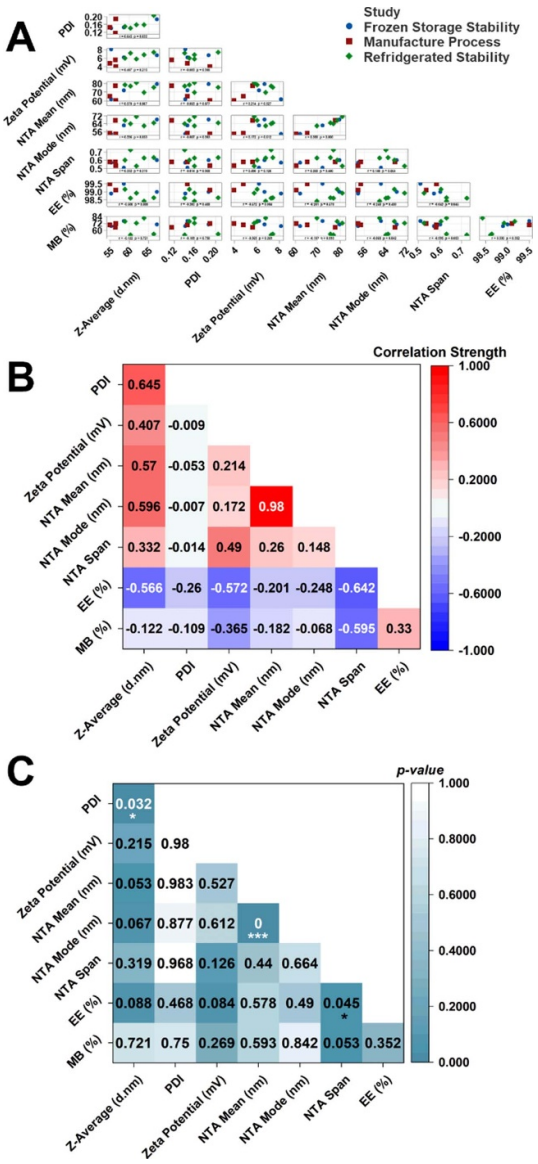

Figure 6. Pearson correlation analysis of inter-batch CQA linear relationship analysis (A) sample grouping distribution and (B) correlation weighting of PolyA DOTAP-LNP CQAs, calculated through division of covariance by compared CQA SD, and (C) correlation significance, $^{*}p < 0.05$, $^{**}p < 0.005$ and $^{***}p < 0.0005$. Zetasizer z-average size and PDI, ELS measured zeta potential, NTA measured mean size, mode size and span, and RiboGreen™ assay for PolyA encapsulation efficiency (EE%), and mass balance recovery (MB%).

range of constituents, screening of prototype formulations during early development is crucial. As the range of academic and industrial applications of LNPs has seen tremendous growth, established techniques within the nanomedicine field have translated into adopted routine techniques for characterising the physicochemical attributes of LNP formulation candidates. Trend analysis of LNP research highlights that novel high-resolution analytical pipelines have not experienced an equivalent growth in their implementation in line with advancements in lipid research and they remain under-utilised for studying prototype formulations (figure 1).

The goal of this study was to apply high-resolution analytical techniques for profiling LNP nanomedicine physicochemical properties during early prototype development to facilitate clinical translation for therapeutic applications. In this work we use DOTAP-LNPs as a model LNP system, using PolyA as a model payload. We report the evaluation of process parameter manufacture and purification steps on LNP physical parameters, and an assessment of their physicochemical stability under refrigerated and ultra-low temperature storage (−80 °C) conditions using increasing-resolution orthogonal techniques. These advanced techniques provide deeper insights into LNP CQAs, enabling better control over CQAs and thereby advancing their translation.

Analysis of process parameter samples demonstrated that post-dialysis exchange of manufacturing buffer to formulation storage buffer resulted in unmasking of surface charges, increasing the LNP particle size

distribution through sub-population formation and decreasing PolyA recovery (table S2). Our results highlight the importance of filter membrane selection. Both the PES and PVDF membranes that were selected were hydrophilic and low-binding: thus, ideally suited to biological aqueous formulated samples. The PVDF membrane contains electronegative fluoride groups, whereas PES contains sulfone moieties. Formulation post-filtration using a PVDF membrane resulted in 73% encapsulation efficiency and loss of 98% of the PolyA drug, compared to the PES membrane with 99% encapsulation and 67% drug recovery. Estimated changes in LNP particle concentration were noted during the manufacturing stages, which would be expected when the LNP formulation is subjected to different process parameters (figure 2(A)). The PES membrane is more suitable for our LNPs than PVDF as the sulfone group is less electronegative than fluoride groups and does not disrupt cationic lipid-PolyA electrostatic interactions. Roces *et al* [9] reported similar DLS z-average increases from post-manufacture to post-dialysis stages, while also reporting a PDI increase from <0.2 to >0.2. The study did not process PolyA-DOTAP-LNPs further by filtration; however, they used a lower molar percentage of DOTAP than our formulation, and different manufacturing operating conditions (TFR 5, 10 and 20 ml min^{-1}, FRR 1:1, 3:1 and 5:1), which could account for the differences noted, as our manufacturing conditions remained constant throughout all batch manufacturing. Ma *et al* [37] screened two- and three-component LNP formulations using DOTAP as the main lipid and a selection of mRNA drugs, which resulted in reported DLS z-averages >200 nm, and zeta potentials of ~ -25 mV.

Our 28 day stability evaluation study under refrigerated conditions highlighted the variable nature of LNP formulations and challenges in defining specifications based on CQA analysis. Zetasizer z-averages showed a gradual increase across 28 days with significant differences in sizes noted at day-7 with an 11 nm increase (table S4). However, DLS inherent bias towards larger particles skewed the results to an overall higher value; contrastingly, no significant size differences were observed with NTA. The zetasizer PDI increased significantly at day 10 and day 14 (table S4), where the NTA span results (table S5) did not significantly change across all evaluated time points. The NTA mean/mode day 10 size values produced were significantly different from other measured time points, as the mean/mode sizes increased without span; these differences indicate equivalent LNP size distributions, with all shifting particle sizes being larger in size. Subsequent time points did not exhibit a significant change in size, demonstrating that methods with higher resolution are not flawless. Stability studies have provided information on formulation changes over a 28 day timeframe (table S4). The literature within the field is extensive on LNP stability; however, with the vastly different prototype formulations used, studies often report conflicting results, with formulations increasing in size over time [38], and other formulation sizes exhibiting stable particle sizes throughout the measurement duration [39, 40].

Current commercial LNP formulations are stored under a variety of conditions, ranging from storage at ambient temperature to refrigerated and frozen conditions. As such, each condition will require buffer excipients to aid with LNP formulation stabilisation throughout the target product shelf life. Here, we used sucrose as a model cryoprotectant and measured the impact of sucrose addition on LNP CQAs using standardised and high-resolution techniques. We noted that the addition of sucrose at 5%–20% (w/v) concentrations in PBS on day 0 did not result in significant alterations in LNP particle size or size distributions when analysing zetasizer and NTA data. Significant differences were noted with the zeta potential (figure 4(C)), PolyA mass balance percentage (table S6) and the initial estimated particle concentration, as measured by NTA (figures 4(E)–(H)). Following freeze/thaw stress induction (storage at -80 °C and subsequent thawing to ambient temperature) produced varied results from day 0.

The DLS-measured parameters highlighted the presence of larger particles accompanied by PDI increases following freeze/thaw stress, with $\geqslant$10-fold increase in size and a 3-fold increase in PDI relative to day 0 (table S6). The LNP formulation containing 10% sucrose produced the lowest size (50 nm), PDI (0.01) and zeta potential (0) differences in comparison to other test conditions. The NTA data were in agreement with the DLS trends, with 10% sucrose producing the highest estimated particle concentration (3×10^{10} particles ml^{-1}) post freeze/thaw (figure 4(G)) of all tested conditions. Across all measured frozen-storage conditions, the NTA mean, mode and span produced less variation in the measured parameters in comparison to DLS. Our results demonstrate sucrose concentrations $>20\%$ are required to prevent F/T-induced agglomeration and ensure formulation stability with a suitable cryoprotectant. Comparison of the size distribution profiles between DLS (figures S3 (A) and (B)) and NTA (figures 4(E)–(H)) demonstrates the need for orthogonal analysis of LNP candidates during the early development, evidenced by NTA detecting stress-induced sub-population formation. Prior work also demonstrates that NTA offers higher-resolution particle size analysis over DLS size measurements in a variety of nanomaterials [41–43].

Beyond the resolution scope of zetasizer DLS and NTA techniques is FFF, a gentle separation technique used to separate and evaluate colloidal size and morphological distributions through hyphenation with

inline MDs. We demonstrate method development for FI-AF4-UV-MALS-DLS and highlight the use of simulations to model formulation distribution outcomes (figure S4). Our AF4 method was developed in accordance with ISO guidelines, ensuring a robust method and reliable results with the criteria noted in table S8, noting high LNP recovery post-AF4 separation and detection, acceptable selectivity and resolution factor. The LNPs analysed on day 0 show two different sized batches of 79 nm (LNP1) and 58 nm (LNP2); each respective batch produced differing UV and MALS detector signals, with LNP1 producing higher detector signal intensities than LNP2. As both batches exhibited high recovery, we could account for the differences in signal to the post-dialysis concentration, and thus a knock-on effect of equivalent AF4 sample prep dilution would further decrease the sample concentration and detector signal intensity. As both batches of LNPs followed equal formulation processes, not all environmental conditions could be controlled due to different laboratory ambient temperatures and lighting. These differences could impact formulation component solubility, stability and miscibility between organic:aqueous phases, thus producing variable outcomes.

Within each batch of LNPs analysed on day 0, multiple peaks are visible in both UV/MALS profiles (figures 5(A) and (B)), highlighting sub-populations present within the overall sample population distribution (figure 5(D)). Freeze/thaw stress induction produced multiple sub-populations within stressed samples, producing low fragmented noisy detector signals for both UV and MALS data. The signals produced were also indicative of 13% sample recovery from separation, denoting that 87% of stressed samples are lost within the AF4 separation and detection process. Prior to AF4 analysis, freeze/thaw stressed LNPs appeared turbid, indicating that sample loss from the freeze/thaw process contributed to poor overall AF4 freeze/thaw sample recovery. Increasing resolution of techniques from DLS to NTA and AF4 demonstrated that stress-induced LNP sub-populations were detected using NTA and AF4 compared to DLS. The main peaks observed in figures 5(E) and (F) occurred at 0.055 ml min^{-1} cross-flow rate, highlighting minimal membrane–aggregate interactions, negligible separation and elution when minimal cross-flow is applied. As LNPs are recovered after NTA, no sample loss is observed using the technique, producing a representative size distribution. Meanwhile, AF4 produced a size distribution reflecting 13% of the injected sample. AF4 indicated morphological impacts of stress on LNPs with visualisation of a broad range of spheres through to rods.

Greawart *et al* [31] manufactured ionisable liposomes containing mRNA and conventional AF4 for separation, and multiplexed with inline small-angle x-ray scattering. While there are few studies reporting the use of AF4 for LNP analysis [11, 13, 30], all these studies have highlighted the need for higher-resolution methodologies for analysing LNP systems using a broader range of components to facilitate routine use of high-resolution methods and AF4 within routine analytical testing of LNPs. The implementation of AF4-MD enables high-resolution analysis of LNPs during early development to identify early developability challenges and facilitate clinical translation.

Our statistical correlations of day 0 LNP formulations post-dialysis without filtration (figure 6) highlight inconsistencies in small-scale batch manufacture, emphasising batch-to-batch variation within LNPs. This was further highlighted through the correlation of physicochemical CQAs measured by routine and high-resolution techniques. For a deeper insight into LNP, global interlaboratory harmonisation efforts and the sharing of larger datasets are needed. Hassett *et al* [24] demonstrate the use of statistical correlations between LNP CQAs; however, due to individual LNP formulation components, these correlation strengths differ from our calculated correlation weightings (figure 6(B)) and statistical significance strengths (figure 6(C)). The LNP CQA statistical correlation approach provides a deeper understanding of the relationship between LNP process design and the associated physicochemical CQAs derived from orthogonal analyes, which can aid bench to bedside translation.

5. Conclusion

We have shown the impact of manufacture, purification and filtration process parameters on formulation physicochemical characteristics. Our refrigerated and ultra-low temperature stability results show the need for high-resolution analytical techniques within early-stage formulation development and AF4 analysis evaluated formulations beyond the scope of adopted routine analytical techniques. This further emphasises the need for high-resolution analytical techniques within routine characterisation of early LNP candidates. For a true representative reference material model, further cryoprotectant or refrigerated storage excipients are required to stabilise formulation CQAs to allow extensive comprehensive use. The AF4 data highlight detectable sub-populations from fresh and freeze/thawed LNP samples, which were undetected using DLS and NTA techniques. Our physicochemical correlation and statistical significance evaluations presented a deeper insight into LNP-associated CQAs, deepening our understanding of formulation behaviour.

Data availability statement

The data that support the findings of this study are openly available at the following URL/DOI: https://doi.org/10.15129/0e076511-618a-45b3-ac43-96c61ed3e6ba. Data will be available from 01 January 2025.

Acknowledgments

This work was supported and funded by the UK Engineering and Physical Sciences Research Council (Z R, EPSRC EP/V028960/1). We acknowledge funding from AstraZeneca Pharmaceuticals for R A's PhD scholarship and the UK Engineering and Physical Sciences Research Council for their support of C G D's PhD scholarship. For the purpose of open access, the authors have applied for a CC BY copyright license to any Author Accepted Manuscript version arising from this submission.

Author contributions

Investigation: C G D, M C, P P, R A, Z R; Methodology: C G D, P P, R A, Z R; Analysis: C G D and Z R; Writing original draft: C G D and Z R; Visualization: C G D; Writing—reviewing and editing: C G D, Y P, R C, K T, R A, N J W R and Z R; Funding acquisition: Z R. All authors have read and agreed to the published version of the manuscript.

Conflict of interest

The authors declare no conflict of interest.

ORCID iDs

Panida Punnabhum https://orcid.org/0009-0002-6830-1072
Michael Cairns https://orcid.org/0009-0006-6759-0190
Robin Capomaccio https://orcid.org/0000-0001-7164-2340
Kevin Treacher https://orcid.org/0000-0002-8705-3476
Zahra Rattray https://orcid.org/0000-0002-8371-8549

References

[1] Robinson E, MacDonald K D, Slaughter K, McKinney M, Patel S, Sun C and Sahay G 2018 Lipid nanoparticle-delivered chemically modified mRNA restores chloride secretion in cystic fibrosis *Mol. Ther.* **26** 2034–46
[2] Fattore L *et al* 2023 Oncosuppressive miRNAs loaded in lipid nanoparticles potentiate targeted therapies in BRAF-mutant melanoma by inhibiting core escape pathways of resistance *Oncogene* **42** 293–307
[3] Qiu M, Li Y, Bloomer H and Xu Q 2021 Developing biodegradable lipid nanoparticles for intracellular mRNA delivery and genome editing *Acc. Chem. Res.* **54** 4001–11
[4] Zhou J-E, Sun L, Liu L, Jia Y, Han Y, Shao J, Wang J, Wang Y, Yu L and Yan Z 2022 Hepatic macrophage targeted siRNA lipid nanoparticles treat non-alcoholic steatohepatitis *J. Control. Release* **343** 175–86
[5] Chen Y *et al* 2022 Lipid nanoparticle-encapsulated VEGFa siRNA facilitates cartilage formation by suppressing angiogenesis *Int. J. Biol. Macromol.* **221** 1313–24
[6] Afonin K A, Dobrovolskaia M A, Church G and Bathe M 2020 Opportunities, barriers, and a strategy for overcoming translational challenges to therapeutic nucleic acid nanotechnology *ACS Nano* **14** 9221–7
[7] Gabizon A A, de Rosales R T M and La-Beck N M 2020 Translational considerations in nanomedicine: the oncology perspective *Adv. Drug Deliv. Rev.* **158** 140–57
[8] Simon C G, Borgos S E, Calzolai L, Nelson B C, Parot J, Petersen E J, Roesslein M, Xu X and Caputo F 2023 Orthogonal and complementary measurements of properties of drug products containing nanomaterials *J. Control. Release* **354** 120–7
[9] Roces C B, Lou G, Jain N, Abraham S, Thomas A, Halbert G W and Perrie Y 2020 Manufacturing considerations for the development of lipid nanoparticles using microfluidics *Pharmaceutics* **12** 1095
[10] Bastogne T, Caputo F, Prina-Mello A, Borgos S and Barberi-Heyob M 2022 A state of the art in analytical quality-by-design and perspectives in characterization of nano-enabled medicinal products *J. Pharm. Biomed. Anal.* **219** 114911
[11] Caputo F, Arnould A, Bacia M, Ling W L, Rustique E, Texier I, Mello A P and Couffin A-C 2019 Measuring particle size distribution by asymmetric flow field flow fractionation: a powerful method for the preclinical characterization of lipid-based nanoparticles *Mol. Pharm.* **16** 756–67
[12] Caputo F, Clogston J, Calzolai L, Roesslein M and Prina-Mello A 2019 Measuring particle size distribution of nanoparticle enabled medicinal products, the joint view of EUNCL and NCI-NCL. A step by step approach combining orthogonal measurements with increasing complexity *J. Control. Release* **299** 31–43
[13] Parot J *et al* 2024 Quality assessment of LNP-RNA therapeutics with orthogonal analytical techniques *J. Control. Release* **367** 385–401
[14] Bost J P *et al* 2021 Delivery of oligonucleotide therapeutics: chemical modifications, lipid nanoparticles, and extracellular vesicles *ACS Nano* **15** 13993–4021
[15] Hammond S M *et al* 2021 Delivery of oligonucleotide-based therapeutics: challenges and opportunities *EMBO Mol. Med.* **13** e13243
[16] Hou X, Zaks T, Langer R and Dong Y 2021 Lipid nanoparticles for mRNA delivery *Nat. Rev. Mater.* **6** 1078–94

[17] Semple S C, Chonn A and Cullis P R 1996 Influence of cholesterol on the association of plasma proteins with liposomes *Biochem.* **35** 2521–5
[18] Patel S *et al* 2020 Naturally-occurring cholesterol analogues in lipid nanoparticles induce polymorphic shape and enhance intracellular delivery of mRNA *Nat. Commun.* **11** 983
[19] Kulkarni J A, Witzigmann D, Leung J, Tam Y Y C and Cullis P R 2019 On the role of helper lipids in lipid nanoparticle formulations of siRNA *Nanoscale* **11** 21733–9
[20] Hald Albertsen C, Kulkarni J A, Witzigmann D, Lind M, Petersson K and Simonsen J B 2022 The role of lipid components in lipid nanoparticles for vaccines and gene therapy *Adv. Drug Deliv. Rev.* **188** 114416
[21] Suzuki T, Suzuki Y, Hihara T, Kubara K, Kondo K, Hyodo K, Yamazaki K, Ishida T and Ishihara H 2020 PEG shedding-rate-dependent blood clearance of PEGylated lipid nanoparticles in mice: faster PEG shedding attenuates anti-PEG IgM production *Int. J. Pharm.* **588** 119792
[22] Ge X, Chen L, Zhao B and Yuan W 2020 Rationale and application of PEGylated lipid-based system for advanced target delivery of siRNA *Front. Pharmacol.* **11** 598175
[23] Moss K H, Popova P, Hadrup S R, Astakhova K and Taskova M 2019 Lipid nanoparticles for delivery of therapeutic RNA oligonucleotides *Mol. Pharm.* **16** 2265–77
[24] Hassett K J, Higgins J, Woods A, Levy B, Xia Y, Hsiao C J, Acosta E, Almarsson Ö, Moore M J and Brito L A 2021 Impact of lipid nanoparticle size on mRNA vaccine immunogenicity *J. Control. Release* **335** 237–46
[25] Choi J, Fuentes C, Fransson J, Wahlgren M and Nilsson L 2020 Separation and zeta-potential determination of proteins and their oligomers using electrical asymmetrical flow field-flow fractionation (EAF4) *J. Chromatogr.* A **1633** 461625
[26] Fuentes C, Choi J, Wahlgren M and Nilsson L 2023 Charge and zeta-potential distribution in starch modified with octenyl succinic anhydride (OSA) determined using electrical asymmetrical flow field-flow fractionation (EAF4) *Colloid Surf.* A **657** 130570
[27] Ramirez L M F, Rihouey C, Chaubet F, Le Cerf D and Picton L 2021 Characterization of dextran particle size: how frit-inlet asymmetrical flow field-flow fractionation (FI-AF4) coupled online with dynamic light scattering (DLS) leads to enhanced size distribution *J. Chromatogr.* A **1653** 462404
[28] Klein M, Menta M, Dacoba T G, Crecente-Campo J, Alonso M J, Dupin D, Loinaz I, Grassl B and Seby F 2020 Advanced nanomedicine characterization by DLS and AF4-UV-MALS: application to a HIV nanovaccine *J. Pharm. Biomed. Anal.* **179** 113017
[29] Velimirovic M, Pancaro A, Mildner R, Georgiou P G, Tirez K, Nelissen I, Johann C, Gibson M I and Vanhaecke F 2020 Joint forces of HR-Spicp-MS and EAF4-MALS for characterization of gold nanorods conjugated with synthetic glycopolymers *The 2nd Int. Online-Conf. on Nanomaterials*
[30] Mildner R, Hak S, Parot J, Hyldbakk A, Borgos S E, Some D, Johann C and Caputo F 2021 Improved multidetector asymmetrical-flow field-flow fractionation method for particle sizing and concentration measurements of lipid-based nanocarriers for RNA delivery *Eur. J. Pharm. Biopharm.* **163** 252–65
[31] Graewert M A *et al* 2023 Quantitative size-resolved characterization of mRNA nanoparticles by in-line coupling of asymmetrical-flow field-flow fractionation with small angle x-ray scattering *Sci. Rep.* **13** 15764
[32] Bian J, Gobalasingham N, Purchel A and Lin J 2023 The power of field-flow fractionation in characterization of nanoparticles in drug delivery *Molecules* **28** 4169
[33] Lou G *et al* 2020 Delivery of self-amplifying mRNA vaccines by cationic lipid nanoparticles: the impact of cationic lipid selection *J. Control. Release* **325** 370–9
[34] Suzuki Y and Ishihara H 2021 Difference in the lipid nanoparticle technology employed in three approved siRNA (Patisiran) and mRNA (COVID-19 vaccine) drugs *Drug Metab. Pharmacokinet* **41** 100424
[35] Gervais C, Grissom C, Little N and Wachoviak M 2010 Cleaning marble with ammonium citrate *Stud. Conserv.* **55** 164–76
[36] Uddin M N and Roni M A 2021 Challenges of storage and stability of mRNA-based COVID-19 vaccines *Vaccines* **9** 1033
[37] Ma X, Wu F, Peng C, Chen H, Zhang D and Han T 2023 Exploration of mRNA nanoparticles based on DOTAP through optimization of the helper lipids *Biotechnol. J.* **18** 2300123
[38] Ball R L, Bajaj P and Whitehead K A 2017 Achieving long-term stability of lipid nanoparticles: examining the effect of pH, temperature, and lyophilization *Int. J. Nanomed.* **12** 305–15
[39] Kamiya M, Matsumoto M, Yamashita K, Izumi T, Kawaguchi M, Mizukami S, Tsurumaru M, Mukai H and Kawakami S 2022 Stability study of mRNA-lipid nanoparticles exposed to various conditions based on the evaluation between physicochemical properties and their relation with protein expression ability *Pharmaceutics* **14** 2357
[40] Muramatsu H, Lam K, Bajusz C, Laczkó D, Karikó K, Schreiner P, Martin A, Lutwyche P, Heyes J and Pardi N 2022 Lyophilization provides long-term stability for a lipid nanoparticle-formulated, nucleoside-modified mRNA vaccine *Mol. Ther.* **30** 1941–51
[41] Hole P *et al* 2013 Interlaboratory comparison of size measurements on nanoparticles using nanoparticle tracking analysis (NTA) *J. Nanopart. Res.* **15** 2101
[42] Ray R M, Hansen A H, Taskova M, Jandl B, Hansen J, Soemardy C, Morris K V and Astakhova K 2021 Enhanced target cell specificity and uptake of lipid nanoparticles using RNA aptamers and peptides *Beilstein J. Org. Chem.* **17** 891–907
[43] Maguire C M, Rösslein M, Wick P and Prina-Mello A 2018 Characterisation of particles in solution—a perspective on light scattering and comparative technologies *Sci. Technol. Adv. Mater.* **19** 732–45